



POLITECNICO
MILANO 1863

SCUOLA DI INGEGNERIA INDUSTRIALE
E DELL'INFORMAZIONE

EXECUTIVE SUMMARY OF THE THESIS

Universal Photonic Processors: Calibration and Operation of a 6-mode Device

LAUREA MAGISTRALE IN ENGINEERING PHYSICS - INGEGNERIA FISICA

Author: NIKI DI GIANO

Advisor: PROF. ROBERTO OSELLAME

Co-advisors: ANDREA CRESPI, FRANCESCO CECCARELLI

Academic year: 2021-2022

1. Introduction

Universal Photonic Processors (UPPs) are photonic integrated devices capable of implementing a programmable arbitrary unitary transformation between the input and output states of light [1].

In the context of an ever-growing need for techniques to realise such circuits, Femtosecond Laser Micromachining (FLM) offers a rapid and cost-effective solution for the fabrication of UPPs with transversal advantages with respect to standard platforms based on planar processes [2]. In FLM, reconfigurability is achieved by fabricating a set of electrical microheaters, deposited over the waveguides, in such a way that the phases of the light signal are modulated by exploiting the thermo-optic effect.

There are two main problems that arise in attempting to operate UPPs. Firstly, as the number of modes at the input of an UPP increases, so does the number of microheaters; it becomes increasingly difficult to calibrate independently the effect of each microheater and operate them effectively in applications. Secondly, if one's aim is to implement unitary transformations, one needs a procedure to retrieve from them the correct microheater settings. Clements et al. [3] de-

veloped an algorithm performing this task, valid for a network with a square layout; the effectiveness of this algorithm has been already demonstrated on circuits fabricated with planar processes [4]. It is however necessary to adapt the algorithm on the FLM platform.

In this work we develop methods to solve these two problems and show experimentally how to implement them in a 6-mode UPP device.

2. Materials and Methods

In this section we describe the 6-mode UPP employed in the work. The topology of the optical circuit is displayed in Fig. 1. In particular, it consists in a network of 15 Mach-Zehnder Interferometers (MZIs) arranged in a square layout [3]. Each MZI features two resistive microheaters deposited on the chip surface, to control its operation. The microheater straddling two directional couplers will be indicated here as *internal shifter* while the other one *external shifter*.

The circuit was fabricated using FLM on Corning EAGLE XG alumino-borosilicate glass at Politecnico di Milano. The length of the chip is 8.5 cm, with 2 cm width and 1.1 mm thickness. The waveguides and the directional cou-

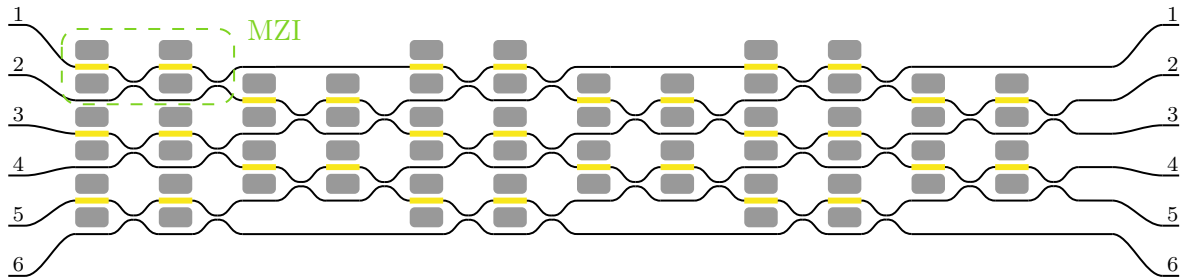


Figure 1: The scheme for the UPPs on which all experiments have been performed. The thin dark lines correspond to FLM waveguides; the yellow thicker lines correspond each to a microheater. Around each microheater is a pair of deep trenches. The group of 2 horizontally aligned directional couplers with microheaters constitutes a reconfigurable MZI of the network.

plers are optimised for a wavelength of 785 nm. The network features six input ports and six output ports. The pitch between ports is $127 \mu\text{m}$, however the inter-waveguide distance inside the network is equal to $80 \mu\text{m}$. Around each microheater there is a pair of $300 \mu\text{m}$ deep trenches for thermal isolation [5], for a total of 60 trenches. The trenches, too, were fabricated with FLM. To connect the microheaters using pins, a pair of printed circuit boards (PCBs) were added. Two copies of this circuit were fabricated with identical specifications, and we shall refer to them as device A and B throughout.

The experimental setup used to calibrate the devices followed the fiber-butt approach: the light signal was provided by two laser sources (793 nm for device A, 785 nm for device B) and coupled through a lens (NA 0.25 coating B) into a 780HP single-mode fiber. The light was coupled from the fiber to the chip by placing the naked fiber near the input ports after peeling and cleaning it.

Finally, the light at the output of the device is collected with an aspheric lens (NA = 0.68 coating B) mounted on a pair of automated stages; these are servo-motors controlled by a C-863 Mercury Servo Controller from Physik Instrumente, providing a positioning repeatability better than $20 \mu\text{m}$. A high repeatability was necessary for the purposes of reliably measuring the same output port on the UPP many times over.

The optical power collected by the output aspheric lens was measured using up to two Ophir NovaII photodetectors connected with Ophir PD300R-IR photodiodes.

In order to control the currents applied to each

of the 30 microheaters on the device, a Qontrol Q8iv Microcontroller setup has been used. On each microheater, the Qontrol Q8iv can provide a current up to 24 mA and a voltage up to 12 V. Python has been used throughout the work for data analysis, curve fitting, automated problem solving as well as controlling the Q8iv and the automated stages.

3. Calibration of the 6-mode UPP

The general transfer matrix of a reconfigurable MZI in the UPP network is given by

$$M(\theta, \phi) = e^{i(\frac{\theta}{2} + \frac{\pi}{2})} \begin{bmatrix} e^{i\phi} \sin(\frac{\theta}{2}) & \cos(\frac{\theta}{2}) \\ e^{i\phi} \cos(\frac{\theta}{2}) & -\sin(\frac{\theta}{2}) \end{bmatrix} \quad (1)$$

where θ and ϕ are respectively the internal and external phases. Each corresponds to a microheater in the physical network (Fig. 1).

Each microheater induces a variable phase change depending on the current I flowing through it; we denote by $\Delta\theta$ an internal phase change and by $\Delta\phi$ an external one. Fabrication tolerances imply that after the fabrication, without the application of any current, there is a random distribution of phases (θ_0, ϕ_0) - which we call *static phases* - for each reconfigurable MZI in the network. Therefore, the internal phase of a reconfigurable MZI is given by $\theta = \theta_0 + \Delta\theta(I)$ (likewise for an external phase).

The electrical power dissipated by a phase shifter heats up the waveguides inducing a change in the refractive index, and the differential change of refractive index is what determines $\Delta\theta$. We assume a model where $\Delta\theta$ depends on the power linearly. The general relation between

power and current is given by $P = RI^2$, where R is the resistance of the device, I is the current. Our experiments show that R is not a constant. This is because the resistivity of metals depends linearly on the temperature in our range of interest, hence it depends on the current. For this reason, our model for $\Delta\theta$ includes a higher order term in the current:

$$\Delta\theta = \alpha I^2(1 + \kappa I^2) = \alpha Q. \quad (2)$$

We introduce the proportionality constant α , called *tuning coefficient*. We can encapsulate the nonlinear current relation into a new variable Q , so that the model for $\Delta\theta$ is linear in this new parameter.

It is important to remark that there is a level of nonlinearity hidden within Q every time we write it, so the conversion from Q to current is not as straightforward as a square root but requires inverting a quadratic function; this quadratic function depends on the microheater in question too, so we have to keep tabs on κ for each microheater.

Finally, the transmission and reflection of an MZI as a function of the internal phase shift θ are given by $\cos^2(\theta/2)$ and $\sin^2(\theta/2)$ respectively [6], so that as a function of the adjusted current square we have

$$\mathcal{T} = \cos^2\left(\frac{\theta_0 + \alpha Q}{2}\right), \quad (3)$$

$$\mathcal{R} = \sin^2\left(\frac{\theta_0 + \alpha Q}{2}\right). \quad (4)$$

In order to extract the values of α , κ and θ_0 for an individual MZI, then, we send an optical signal to only one input port of the MZI; then, we increase the current over time and we measure one of the outputs and perform a curve fit on the data. By convention we always measure the output that corresponds to transmission. We refer to this operation as *calibrating a phase*.

3.1. Calibration of Internal Phases

The real challenge of calibrating the circuit lies in decoupling the effect of every single MZI in the network from all others. In the literature we can find a method to sequentially calibrate each internal phase for a triangular layout [7]; we took it as a starting point in this work and

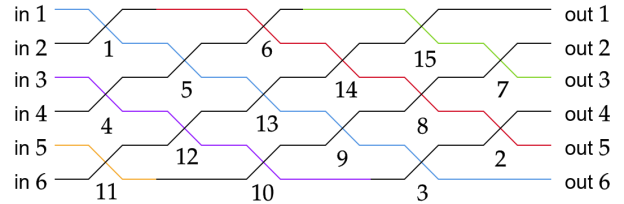


Figure 2: The compact version of the diagram of the 6-mode UPP with the diagonals highlighted.

developed a method for the case of a square layout, which we now describe.

The basic idea of the method is to calibrate the circuit by diagonals (Fig. 2). In fact, after performing an internal phase calibration on an MZI successfully, it is possible to set the current on the MZI so that its transmission becomes unitary; at that point, the optical signal is transferred to the next MZI down the diagonal and the process can start again.

For the 6-mode UPP, we couple laser light into input 1 and measure the optical power out of output 6, then we perform the calibration of the diagonal as described above. The next step is to set the current on MZI 1 such that the reflection \mathcal{R} is equal to 1, and set the power meter to measure output 5. At this point we can calibrate the entire upper diagonal. After this, we can set MZI 6 to unitary reflection, the output to port 3, and calibrate the last diagonal in the same way.

Finally, we set the power meter to output 6 for the rest of the procedure. We change the input from 1 to 3 and set MZI 3 to unitary reflection and we calibrate the first lower diagonal. At the end of this process, we set MZI 10 to unitary reflection. Finally, we change the input from 3 to 5 and calibrate the last diagonal consisting of only MZI 11.

At the end of this process we have obtained α , κ and θ_0 for all the internal phases.

3.2. Thermal Cross-Talk

In a general operation of the circuit, it is necessary to actuate multiple adjacent microheaters. As explained by Ref. [5], the reconfiguration of an MZI through the thermo-optic effect induces a phase shift not only on the MZI of interest but on all other neighboring MZIs by thermal cross-talk. In a more comprehensive model, then, the value θ_i for the i -th MZI depends on every single

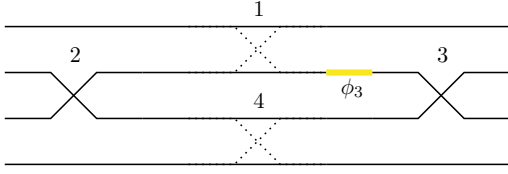


Figure 3: An interferometric loop. The dotted crossings represent MZIs that have been set to unitary reflection. The crossings with a thick bar represent MZIs that have been set to the $\theta = \pi/2$ point, where they behave as balanced directional couplers. The thick yellow line represents the external microheater ϕ_3 of MZI 3.

MZI in the network:

$$\theta_i = \theta_{i0} + \sum_{j=0}^N \alpha_{ij} Q_j. \quad (5)$$

Therefore, the tuning coefficient α is now a *tuning matrix* with entries α_{ij} . The diagonal elements of the tuning matrix α_{ii} are just the values of α obtained at the end of the calibration process.

Measuring the diagonal element α_{ik} amounts to calibrating the internal phase of MZI i but we increase the current on the internal microheater of MZI k instead of MZI i . Moreover, to make the curve fit more accurate, we measure both output ports of MZI i and normalise the power output.

Our measurements show that the off-diagonal tuning elements are cut down by a factor 20%-30% the further away we look from the i -th MZI. This means that for devices with many modes it is not necessary to measure all the elements of the matrix, as eventually the value becomes negligible. Therefore, the cross-talk measurement process is scalable since the number of measurements is $O(N)$ with N number of input ports.

3.3. Calibration of External Phases

Finding all the cross-talk coefficients allows one to operate all internal phases simultaneously; this means that the circuit can now simulate an optical setup with mirrors and beam splitters. Because of this, it is possible to calibrate the external phases by enclosing them in interferometric loops, for example as in Figure 3. These loops behave like an MZI and can therefore be calibrated in the same way as we did for the internal phases, extracting ϕ_0, κ and α for

almost every external phase.

As it turns out, only 10 out of 15 external phases can be characterised through this method; fortunately, the remaining 5 are irrelevant for the purposes of operating the device. The external phases of MZI 1, 4, 11 (Fig. 2) act as global phases in our measurement setup and can therefore be ignored; MZI 5 and 12 can be assumed to have zero external static phase.

4. Operation of the 6-mode UPP

Operating an UPP amounts to choosing the vector $\varphi = (\theta, \phi)$, where θ and ϕ are the arrays of internal and external phases for each MZI in the network respectively.

In case one aims to implement a target unitary matrix \mathbf{U}_T , however, a procedure is required to obtain the vector φ starting from the target unitary matrix. In the literature we can find Clements' algorithm [3]; this procedure decomposes the target \mathbf{U}_T into a multiplication of elementary matrices, each of which corresponds to an MZI of the network of the UPP. From this we can extract the internal and external phases that the MZIs need to have in order to implement the target unitary and thus determine φ . We can group the static phases into another vector φ_0 ; we can then proceed to find the Q_i by inverting Eq. 5. Simply inverting it however would not ensure that the resulting Q_i are positive, which is required by their physical meaning as squared currents; for this reason we leverage the fact that the behavior of an MZI is 2π -periodic in both θ and ϕ (Eq. 1). Therefore it suffices to add or remove multiples of 2π from φ until all entries of the solution vector \mathbf{Q} are positive. In other words, the problem becomes:

$$\begin{aligned} & \text{minimize} && \sum_i Q_i \\ & \text{subject to} && Q_i \geq 0 \quad \forall i \quad \text{and} \\ & && \alpha \mathbf{Q} + 2\pi \mathbf{n} = \varphi - \varphi_0. \end{aligned} \quad (6)$$

Here \mathbf{n} is a vector of integers of the appropriate dimensions. The problem mixes integer variables and real variables, making it a Mixed Integer Linear Programming (MILP) problem, which we solved using the GEKKO library for Python.

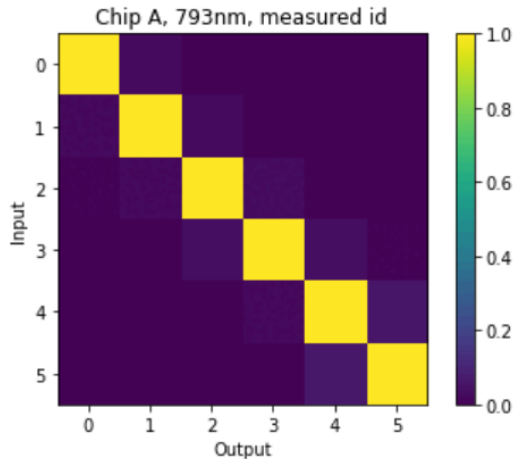


Figure 4: The identity matrix implemented using device A at 793 nm. The fidelity of this implementation is 0.99856.

4.1. Results of the Experiments

Using the machinery developed so far we implemented unitary matrices on A and B. We divided the results in two different sets: *Switching* matrices, and *Haar Random* matrices. In order to measure the performance of the devices we used the *absolute fidelity* $\overline{\mathcal{F}}(\mathbf{U}_{\text{meas}}, \mathbf{U}_T) = \sum_{ij} |U_{ij,\text{meas}}| |U_{ij,T}|$. Our experimental setup indeed allows to retrieve the absolute value of the experimental matrix entries.

The Switching matrices can be obtained without operating external phases and have either 0 or 1 as entries. The Switching set we implemented contains 21 matrices: the matrix that cycles clockwise any input (meaning that $1 \rightarrow 2, 2 \rightarrow 3, \dots, 6 \rightarrow 1$) and all the powers of this matrix, which we call *Pauli set*; five matrices that swap input 2 with any other output keeping the other inputs the same, which we call *Port Swap set*; moreover, it contains ten randomly chosen permutation matrices. The performance of both devices on the Switching set is summarised in Table 1; an example of implemented matrix is shown in Fig. 4.

For the Haar Random set, 57 matrices were implemented but only on device A. The fidelity on this set was 0.89076 ± 0.04660 and the distribution is shown in Fig. 5.

The sharp drop in fidelity when dealing with Random Haar matrices, which differ by switching matrices primarily because they employ external phases in addition to internal ones, suggests that we have room for improvement in im-

Matrix Set	$\overline{\mathcal{F}}_A$ (793 nm)	$\overline{\mathcal{F}}_B$ (785 nm)
Pauli	0.99538 ± 0.00196	0.99669 ± 0.00053
Port Swap	0.99709 ± 0.00066	0.99695 ± 0.00050
Random	0.99363 ± 0.00101	0.99673 ± 0.00051
Total	0.99537 ± 0.00077	0.99679 ± 0.00030

Table 1: The fidelities measured on the three different sets of switching matrices. The data reported here is the average fidelity and standard deviation over the set.

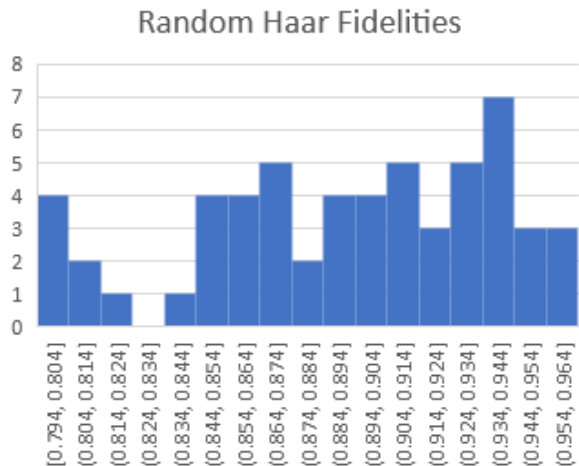


Figure 5: The distribution of the fidelities obtained from the 57 measured Haar.

plementing the external phase control.

4.2. Common Mode Phase

One problem behind the control of the random Haar matrices can be traced back to the very model that has been used to decompose the original unitary matrix in Clements' algorithm. Indeed in the original work by Clements the common mode phase $\phi_{\text{com}} = \theta/2 + \pi/2$ (Eq. 1) is not taken into account.

Typically when considering an MZI by itself this common mode phase can be ignored, however inside a network this phase has a substantial effect on the external phases. Therefore, when operating the circuit after retrieving the vector φ we need to perform a remapping of the external phases in order to reflect the effects of this common mode phase. Indeed, for a given external phase there are always up to two MZIs that influence it with their common mode phase: one adds an extra unwanted phase, the other subtracts a phase. Therefore, using the numbering from Fig. 3 as reference the new external phase

of MZI 3 would be given by

$$\phi'_3 = \phi_3 - \left(\frac{\theta_1}{2} + \frac{\pi}{2}\right) + \left(\frac{\theta_4}{2} + \frac{\pi}{2}\right) \quad (7)$$

where we keep the constant factors even though they would cancel out. If MZI 1 or 4 were missing, for example at the edges of the UPP network, these factors would not cancel out so we report them for completeness.

We now move to analysing the effects of thermal cross-talk on the common mode phase. As a matter of fact, using the thermo-optic effect we induce a differential phase shift on the waveguide which determines the variable phase $\Delta\theta$. However, we also induce a common phase shift on the waveguides, because the microheaters heat up both waveguides at once. Because of this effect, we need to add two extra terms to the common mode phase:

$$\phi_{\text{com}} = \frac{\theta}{2} + \frac{\pi}{2} + \beta\theta + \gamma\phi. \quad (8)$$

The parameters β and γ are new tuning coefficients that need to be measured for each MZI. It is possible to measure β and γ using the same interferometric loops as in Fig. 3. We performed these measurements only on one MZI in the network, yielding a $\beta = 0.17$; this means that the influence of cross-talk is about 34% in air, which is consistent with the findings on thermal cross-talk between different MZIs.

5. Conclusions

Throughout this work we discussed Universal Photonic Processors (UPPs), devices capable of implementing an arbitrary unitary transformation between quantum states of light. We introduced a method to calibrate an UPP device fabricated with the FLM platform, taking into account the nonlinearity of the resistance for the microheaters as well as the effect of the thermal cross-talk between adjacent MZIs. We used this calibration procedure on the 6-mode UPP, demonstrating a fidelity of 0.99536 ± 0.00077 on the Switching set which is better than the current state of the art [4]. On the Haar random set the fidelity was 0.89076 ± 0.04660 which is comparable to the state of the art, yet with room for improvement.

Our data show that a more refined model is

needed for the operation of the UPP. We proposed a more refined model that includes the effects of thermal cross-talk and showed experimental evidence that these effects are relevant for the operation of the UPP.

In the future we expect to carry out a new measurement of Haar Random matrices using a complete calibration of the refined model. The excellent performance of the device on the Switching set make us envisage that similar fidelities can be achieved on the Haar Random set also, and our aim for the future is to confirm experimentally these indications.

References

- [1] W. Bogaerts *et al.*, “Programmable photonic circuits,” *Nature*, vol. 586, pp. 207–216, Oct. 2020.
- [2] G. Corrielli *et al.*, “Femtosecond laser micromachining for integrated quantum photonics,” *Nanophotonics*, vol. 10, pp. 3789–3812, Nov. 2021.
- [3] W. R. Clements *et al.*, “Optimal design for universal multiport interferometers,” *Optica*, vol. 3, pp. 1460–1465, 2016.
- [4] C. Taballione *et al.*, “A universal fully reconfigurable 12-mode quantum photonic processor,” *Materials for Quantum Technology*, vol. 1, p. 035002, 8 2021.
- [5] F. Ceccarelli *et al.*, “Low Power Reconfigurability and Reduced Crosstalk in Integrated Photonic Circuits Fabricated by Femtosecond Laser Micromachining,” *Laser & Photonics Reviews*, vol. 14, no. 10, p. 2000024, 2020.
- [6] R. G. Hunsperger, *Integrated Optics, Theory and Technology*. Springer, 6 ed., 2009.
- [7] J. Carolan *et al.*, “Universal linear optics,” *Science*, vol. 349, no. 6249, pp. 711–716, 2015.